Structural and mechanistic basis for RiPP epimerization by a radical SAM enzyme

Xavier Kubiak, Ivan Polsinelli, Leonard Chavas, Cameron Fyfe, Alain Guillot, Laura Fradale, Clémence Brewee, Stéphane Grimaldi, Guillaume Gerbaud, Aurélien Thureau, et al.

Editor summary:

Peptide epimerization is a common but enigmatic post-translational modification found in antibiotics formed from ribosomally-synthesized and post-translationally modified peptides. Now, crystallographic snapshots, spectroscopy and biochemical investigations, have provided insight into the mechanism of peptide epimerization catalyzed by radical SAM epimerases.

Peer Review Information:

Nature Chemical Biology thanks Qi Zhang and the other, anonymous reviewers for their contribution to the peer review of this work.

1. Extended Data

Figure or Table # Please group Extended Data items by type, in sequential order. Total number of items (Figs. + Tables) must not exceed 10.	Figure/Table title One sentence only	Filename Whole original file name including extension. i.e.: Smith_ED_Fig1.jpg	Figure/Table Legend If you are citing a reference for the first time in these legends, please include all new references in the main text Methods References section, and carry on the numbering from the main References section of the paper. If your paper does not have a Methods section, include all new references at the end of the main Reference list.
Extended Data Fig. 1	**Topology diagram of EpeE, radical SAM binding motifs and coordination of SAM in EpeE and representative members of the radical SAM enzyme superfamily**.	ED_Figure1.jpg	**a,** EpeE topology diagram showing a truncated α5/β6 TIM barrel in the radical SAM domain and T-SPASM domain with a single AuxI cluster. The binding region is depicted in bold line. The position of the [4Fe-4S] clusters (yellow and orange) and the coordinating cysteine residues (yellow) are indicated. **b,** Radical SAM cluster of EpeE in interaction with SAH. Residues from the conserved: GGE, GXIXGXXE, ribose, β6 and $CX_3CX\Phi C$ motifs are colored according to their domain in EpeE (radical SAM domain). The unusual His-20 residue from the $CX_3CX\Phi C$ motif is highlighted. Hydrogen-bonds are shown with black lines, radical SAM [4Fe-4S] cluster with yellow and orange sticks and SAH with green sticks. **c,** The $CX_3CX\Phi C$ motif of structurally characterized members of the radical SAM superfamily of enzymes. The Φ residue is: Tyr in AnSME (green sticks) and CteB (brown sticks); Phe in SkfB (yellow sticks) and SuiB (violet sticks); Met

			in NosL (white sticks). As for CteB, the side chain of the Φ amino acid coordinates both the adenine and the ribose moiety, but only EpeE makes two H-bonds with the N6 and N7 of the adenine moiety.
Extended Data Fig. 2	**Interactions stabilizing the T-SPASM domain and the bridging region of EpeE.**	ED_Figure2.jpg	**a,** Overall structure of EpeE highlighting the bridging region (red cartoon) between EpeE domains (radical SAM domain in light blue, T-SPASM in teal). **b,** The bridging region (red cartoon) makes extensive H-bonds (black dotted lines) with α3' helix and α3'-α4' loop (green cartoon) (left panel). The C-terminal helix α5' is stabilized by α3' helix through H-bond and hydrophobic interactions (right panel). **c,** Comparison between the twitch and SPASM-domains of representative radical SAM enzymes. Similarly to twitch radical SAM enzymes (SkfB & BtrN), EpeE coordinates a single [4Fe-4S] cluster, however, the bridging region extends toward the location of AuxII cluster found in SPASM enzymes (AnSME, CteB & SuiB). The *C*-terminal α5' helix of EpeE, absent in twitch-domains, is displaced at the opposite side of the AuxI cluster compared to the C-terminal α6' helix of SPASM-domain enzymes AnSME and CteB which lies against the α6 helix of the TIM barrel (missing in EpeE). Only the AuxI cluster, β1'-β2' anti-parallel sheets and α2' helix positions are conserved in all enzymes. The TIM barrel domain is colored in white. The Twitch/SPASM domains are colored by protein. The AuxI and II clusters are shown in yellow and orange sticks.
Extended Data Fig. 3	**EPR, UV-visible and HYSCORE analysis of EpeE in absence or presence of SAM.**	ED_Figure3.jpg	**a,** Temperature dependence of EPR spectra of dithionite-reduced reconstituted samples of wild-type EpeE in the absence (left panel) or in the presence (right panel) of a 5-fold stoichiometric excess of SAM. The microwave power was adjusted at each temperature to avoid saturation effects. Spectra have been amplitude-normalized. Number of accumulations: 4. The signal of the SAM-bound $[4Fe\text{-}4S]^{+}$ cluster relaxes significantly faster than the one detected in the unbound form. Indeed, the former broadens at temperatures above 6 K and is no longer visible at 30 K and above (right panel) whereas the latter is still detected without significant broadening at 30 K (left panel). Such differences in the relaxation behavior of the two forms allowed us to reveal partial conversion between these forms upon addition of SAM. Indeed, a weak contribution of the unbound form is detected in the sample incubated with a 5-fold excess of SAM when measured at 30 K (right panel). **b,** Power saturation experiments of dithionite-reduced reconstituted samples of wild-type EpeE in

			the absence (upper panel) or in the presence (lower panel) of a 5-fold stoichiometric excess of SAM. Peak-to-peak amplitudes between features measured as indicated by arrows on left spectra are plotted against square root of microwave power in a log-log plot (blue filled circles). The dotted line represents the non-saturation regime for which the EPR amplitude is proportional to the square root of the microwave power. Other experimental conditions: temperature, 15 K (upper panel) or 6 K (low panel), microwave power, 0.1 mW (left spectra), number of accumulations, 4. **c,** UV visible analysis of EpeE wild-type (upper panel) and A3-mutant (lower panel). Before (grey line) and after (black line) anaerobic FeS cluster reconstitution. **d,** X-band HYSCORE spectra of dithionite-reduced reconstituted samples of wild-type EpeE in the presence (upper panel) or in the absence (lower panel) of a 5-fold stoichiometric excess of SAM. Only the low frequency region is shown. Experimental conditions are given in the Methods section. The low frequency region of the HYSCORE spectrum of the anaerobically reduced and reconstituted wild type enzyme in the presence of SAM displays a complex set of signals in both the (+, +) and (-, +) quadrants which can be unambiguously assigned to a hyperfine coupling to a ^{14}N nucleus in the intermediate coupling regime for which the isotropic part of the hyperfine coupling constant a_{iso} is nearly equal to twice the ^{14}N Larmor frequency, i.e. $\nu_I(^{14}N) \approx 1.1$ MHz (upper panel). These signals are absent in the corresponding HYSCORE spectrum of the enzyme prepared in the same conditions but without SAM (lower panel).
Extended Data Fig. 4	**LC-MS analysis of EpeE incubated with peptides 4, 5, 6 & 7.**	ED_Figure4.jpg	Activity of EpeE with peptide **4** (**a**), **5** (**b**), **6** (**c**) and **7** (**d**) was assayed in deuterated buffer. LC-MS analysis of peptide at T0 (upper left panel) and after 90 min incubation under anaerobic conditions (lower left panel). Comparison between the mass spectrum of the substrate (upper middle panel) and the product (lower middle panel) showed a +1 Da mass increment, consistent with ^{2}H-atom incorporation while mass spectrum analysis of the 5'-dA is shown in right panel.
Extended Data Fig. 5	**LC-MS/MS analysis of the peptide 4, 5, 6 and 7 and the reaction products formed after**	ED_Figure5.jpg	**a,** Mass fragmentation spectrum of peptide **4** (upper panel) and the epimerized peptide product (lower panel). (***see Supplementary Tables 1 - 2 for full assignment***). **b,** Mass fragmentation spectrum of peptide **5** (upper panel) and the epimerized peptide product (lower panel). (***see Supplementary Tables 3 - 4 for full assignment***). **c,** Mass fragmentation

	incubation with EpeE.		spectrum of peptide **6** (upper panel) and the epimerized peptide product (lower panel). (***see Supplementary Tables 5 - 6 for full assignment***). **d,** Mass fragmentation spectrum of peptide **7** (upper panel) and the epimerized peptide product (lower panel). (***see Supplementary Tables 7 - 8 for full assignment***). The relevant ions with a mass shift of +1 Da due to ^{2}H incorporation after reaction with EpeE are highlighted.
Extended Data Fig. 6	**Comparison between substrate-free and peptide-bound structures of EpeE.**	ED_Figure6.jpg	**a**, Superimposition of substrate-free and peptide-bound structures of EpeE. **b**, Close-up view showing the major structural movements including the α3'-α5' helices (indicated by arrows in panel a) of the SPASM-related domain. The substrate-free EpeE structure is shown in grey and the peptide-bound EpeE structure in pale cyan (chain A) and deep teal (chain B). Alignment of the substrate-free and -bound structures using all domains (634 residues) has a r.m.s.d. of 0.78 Å, as calculated using Coot SSM.
Extended Data Fig. 7	**Peptide 5 bound in the active-site of wild-type EpeE structure.**	ED_Figure7.jpg	**a,** The peptide **5** was built for 7 out of 11 residues (KENRWIL) according to the electron density. The omit map (blue mesh) of peptide **5** (in pink sticks) is contoured at 3σ. SAH is depicted in stick, the radical SAM [4Fe-4S] and AuxI clusters are shown as spheres. **b,** Peptide **5** fold. The peptide is shown in salmon (chain C) and orange (chain D) and colored by atom type. Intramolecular interactions are depicted in black dashed line.
Extended Data Fig. 8	**Structures of C223A EpeE mutant bound with peptide 5 and 6.**	ED_Figure8.jpg	**a,** Superimposition of EpeE WT in complex with peptide **5** (pale cyan) and EpeE **C223A** in complex with peptide **5** (bright orange; r.m.s.d. of 0.22 Å). **b,** Superimposition of EpeE WT in complex with peptide **5** (pale cyan) and EpeE **C223A** in complex with peptide **6** (green; r.m.s.d. of 0.23 Å). **c,** Close-up of EpeE **C223A** mutant active site. The peptide **5** (left panel) was built for 9 out of 11 residues (KSKENRWIL) according to the electron density. The peptide **6** (right panel) was built for all the 11 residues (KENRWILGSGH) according to the electron density. The omit maps (blue mesh) of peptide **5** (pink sticks) and **6** (purple sticks) are contoured at 3σ. SAH (green) is depicted in stick, the radical SAM [4Fe-4S] and AuxI clusters are shown as spheres. **d,** Structure of EpeE C223A mutant with peptide 6 in its active site. K171 and D143 are

			stacking H49 from peptide **6** (left panel) while, in the substrate-free WT EpeE structure, D143 and K171 have a distinct orientation stabilized by a salt bridge (right panel). **e,** The presence of H49 in the structure of EpeE C223A mutant with peptide 6 provided inter-chain interactions between the two enzyme subunits.
Extended Data Fig. 9	**The C223 residue in the structures of wild-type EpeE and D210A mutant.**	ED_Figure9.jpg	**a,** Interactions involving D210 in the structure of EpeE with peptide **5**. D210 provides key electrostatic interactions to the substrate (residues N41 and R42) and is stabilized by a polar bond with the protein residue T5. The distance between C223 and D210 is 5.08 Å. **b, Orientations of C223 in the structure of the D210A EpeE mutant.** The omit map (blue mesh) of C223 in chain A (left panel) and chain B (right panel) is contoured at 3σ. C223 was modeled as a persulfurated cysteine residue. In chain A (left panel), C223 adopted two orientations.
Extended Data Table. 1	**Crystallographic data and refinement statistics**	Table_1.pdf	

1. Supplementary Information:

A. PDF Files

Item	Present?	Filename Whole original file name including extension. i.e.: Smith_SI.pdf. The extension must be .pdf	A brief, numerical description of file contents. i.e.: *Supplementary Figures 1-4, Supplementary Discussion, and Supplementary Tables 1-4.*
Supplementary Information	Yes	Supplementary_Information.pdf	Supplementary Tables 1-10

Reporting Summary	Yes	nr-reporting-summary.pdf
Peer Review Information	No	*OFFICE USE ONLY*

2. Source Data

Parent Figure or Table	Filename Whole original file name including extension. i.e.: *Smith_SourceData_Fig1.xls,* or *Smith_ Unmodified_Gels_Fig1.pdf*	Data description i.e.: Unprocessed western Blots and/or gels, Statistical Source Data, etc.
Source Data Fig. 4	Source_data_file.csv	Statistical source data for Fig. 4b

Structural and mechanistic basis for RiPP epimerization by a radical SAM enzyme

Xavier Kubiak[1+], Ivan Polsinelli[1+], Leonard M. G. Chavas[3+], Cameron D Fyfe[1+], Alain Guillot[1], Laura Fradale[1], Clemence Brewee[1], Stéphane Grimaldi[4], Guillaume Gerbaud[4], Aurélien Thureau[2], Pierre Legrand[2], Olivier Berteau[1]* & Alhosna Benjdia[1]*

[1]Université Paris-Saclay, INRAE, AgroParisTech, Micalis Institute, ChemSyBio, 78350 Jouy-en-Josas, France
[2]Synchrotron SOLEIL, HelioBio group, L'Orme des Merisiers, 91190 Gif sur-Yvette, France
[3]Nagoya University, Nagoya 464-8603, Japan.
[4]Aix Marseille Univ, CNRS, BIP, IM2B, IMM, Marseille, France

*Corresponding authors. Email: Olivier.Berteau@inrae.fr; Alhosna.Benjdia@inrae.fr

[+]Equal contribution

D-amino acid residues have been reported in countless peptides and natural products including ribosomally-synthesized and post-translationally modified peptides (RiPPs), where they are critical for the bioactivity of several antibiotics and toxins. Recently, radical S-adenosyl-L-methionine (SAM) enzymes have emerged as the only biocatalysts

capable of installing direct and irreversible epimerization in RiPPs. However, the mechanism underpinning this biochemical process is ill-understood and the structural basis for this post-translational modification remains unknown. Here we report an atomic-resolution crystal structure of a radical SAM RiPP-modifying enzyme in complex with its substrate properly positioned in the active site. Crystallographic snapshots, SEC-SAXS, EPR spectroscopy and biochemical analyses revealed how epimerizations are installed in RiPPs and support a unprecedented enzyme mechanism for peptide epimerization. Collectively, our study brings unique perspectives on how radical SAM enzymes interact with RiPPs and catalyze post-translational modifications in natural products.

Introduction

Ribosomally-synthesized and post-translationally modified peptides (RiPPs) form one of the major families of natural products[1,2]. They have recently attracted considerable interest because of their involvement in the homeostasis of the human microbiota[2-6] and their potential to develop innovative antibiotics[7-9]. The biosynthesis of RiPPs usually follows a simple logic with the translation of a precursor peptide containing a leader or a follower sequence[2] which is recognized by tailoring enzymes *via* a specific domain called RRE (RiPP precursor peptide recognition element)[10]. After modification, the leader sequence is cleaved off and the modified peptide secreted. If the general principles are well established, how post-translational modifications are installed and precursor peptides recognized by biosynthetic machineries remains largely elusive[1,2].

Among the broad diversity of RiPP post-translational modifications, epimerization has been only marginally investigated. In eukaryotes, the L-to-D conversion of peptide residues is critical for the activity of various toxins, venoms and neuro-peptides[11]. However, the catalytic processes underpinning these transformations are largely unknown. In prokaryotes, the combined action of a dehydratase and a reductase has been shown to result in the conversion of L-Ser and L-Thr into D-Ala and D-α-aminobutyrate, respectively[12,13]. However, not only this transformation is restricted to Ser and Thr residues but it leads to the modification of the nature and reactivity of the amino acid side-chain.

Recently, novel RiPP families including proteusins[14] and epipeptides[9] have been shown to contain D-amino acid residues formed by the direct and irreversible epimerization of L-residues[2,9,14,15]. *In vivo* and *in vitro* studies have demonstrated that epipeptides induce the expression of LiaRS, a two-component system that orchestrates the cell envelope stress response in *Bacillus subtilis*[16-18]. This system, highly conserved among Firmicutes, regulates the expression of various genes involved in oxidative stress and cell wall antibiotic responses[17-19]. We have shown that the activity of epipeptides is strictly dependent on the presence of epimerized residues[9] (**Figs. 1a, b**) and established that they have a distinct mode of action compared to other known antimicrobial peptides[18]. In addition, we have demonstrated that epipeptides are widely distributed in the human microbiota[9,17,18] and that epimerizations are catalyzed by a radical *S*-adenosyl-L-methionine (SAM or AdoMet) enzyme called EpeE[9,17]. Radical SAM enzymes are central biocatalysts in RiPPs biosynthesis and have been shown to install an outstanding diversity of post-translational modifications[4,5,8,20-26]. However, until now, no radical SAM enzyme has been crystallized in complex with its peptide substrate properly positioned in the active site, limiting our understanding of their catalysis.

To decipher how radical SAM enzymes introduce post-translational modifications in RiPPs and catalyze epimerization, we have performed EPR, SEC-SAXS and structural analysis of the radical SAM epimerase EpeE from *B. subtilis*[9,17]. We circumvented the intrinsic difficulty to obtain RiPP-enzyme complexes by developing a RiPP-fragment based approach combined with targeted mutagenesis. This novel approach allowed to get at a high resolution, the first crystal structure of a RiPP-modifying radical SAM enzyme in interaction with its substrate. We have also solved the structure of several EpeE mutants and trapped an unexpected adduct on a reactive cysteine residue. Collectively, our work provides a structural and mechanistic rationale for peptide epimerization, a rare case of redox-neutral reaction catalyzed by radical SAM enzymes.

Results

EpeE, a RiPP radical SAM enzyme with a truncated TIM barrel

We crystallized EpeE anoxically in the presence of the *S*-adenosyl-L-methionine (SAM) or *S*-adenosylhomocysteine (SAH) cofactor. No significant structural difference was measured (r.m.s.d value of 0.293 Å) however, in subsequent experiments SAH gave high-resolution structures when co-crystallization was performed with peptide substrates. The structure of EpeE with SAH, featuring a homodimer in the asymmetric unit, was determined at resolution of 2.4 Å (**Fig. 1c**). Out of the 319 protein residues, electron density was observed for residues 1 to 317 in both chains. EpeE exhibits several unique features: first, it is built on a truncated radical SAM domain consisting of an *N*-terminal partial triose-phosphate isomerase (TIM) barrel fold (*i.e.* β6/α5) instead of the canonical (β/α)6 TIM barrel. Only the radical SAM enzymes QueE[27] and BtrN[28], which modify small organic substrates, exhibit a shorter core domain (*i.e.* a β6/α3 and β5/α4 partial TIM barrel, respectively). Second, EpeE is devoid of the α4a helix connecting β4-sheet to α4-helix and found in all structurally characterized RiPP-modifying radical SAM enzymes[29,30] (**Extended Data Fig. 1a**). Among the radical SAM motifs, we identified the three cysteine residues (C14, C18 and C21) as coordinating the radical SAM [4Fe-4S] cluster with SAH bound, as expected, to the unique iron-atom through its carboxy and amino groups (**Fig. 1d**). The SAH ligand was further stabilized by the conserved GGE, ribose, "GXIXGXXE" and β6 motifs (**Extended Data Fig. 1b**)[31]. However, in the $CX_3CX\Phi C$ motif, the Φ residue is not an aromatic residue but H20 which coordinates both N6 and N7 from the adenine moiety and unexpectedly stabilizes the ribose moiety *via* side-chain H-bond with O2' (**Extended Data Fig. 1b-c**). Finally, the GGE motif also contains a non-proline *Cis*-peptide bond between the two glycine residues.

A *C*-terminal domain with an unusual architecture

As a hallmark, radical SAM enzymes involved in peptide or protein post-translational modifications have been shown to possess a *C*-terminal domain housing additional iron-sulfur clusters. This *C*-terminal domain is either between 106-115 residues long with two auxiliary iron-sulfur clusters and called a SPASM domain[29,30,32,33], or significantly shorter and unstructured with a single iron-sulfur cluster and called a twitch domain[34]. Single anomalous diffraction at the peak absorption wavelength of iron was consistent with the presence of four iron-sulfur clusters in the EpeE dimer (**Extended Data Table 1**). Besides the radical SAM [4Fe-4S] cluster, a single auxiliary cluster (AuxI), best accounted for by a [4Fe-4S] cluster and fully ligated by four cysteine residues (C206, C222, C289 and C292) was identified (**Fig. 1d**). Two of these 4 cysteine ligands are flanking the conserved β-hairpin while the other two are localized in the α4' helix. This iron-sulfur cluster, located at 16.9 Å from the radical SAM cluster, belongs to the *C*-terminal domain which overall length (111 residues) unexpectedly exceeds the size of a twitch domain. In addition, the β6-β1' bridging loop makes extensive H-bond interactions with the α3' helix and the α3'- α4' loop and extends toward the location where the second cluster is found in SPASM domains (**Extended Data Fig. 2**)[35]. Additional helices (α3', α4', α5'), absent in twitch domains and involving a tight H-bond network, π-π stacking and hydrophobic interactions, are also present establishing a unique and high secondary structure organization (**Extended Data Fig. 1a, 2**). Overall, the EpeE structure blurs the demarcation between SPASM and twitch domains and defines a transient architecture that we propose to call a T-SPASM domain.

EPR spectroscopic characterization of EpeE

To investigate the properties of the two iron-sulfur clusters, we analyzed EpeE by EPR spectroscopy. The EPR spectrum of EpeE, after reconstitution and reduction, showed a single paramagnetic component characterized by an axial shape with *g*-values $g_{\parallel}$ = 2.036 and $g_{\perp}$ = 1.929, which are typical for a reduced *S* = ½ radical SAM [4Fe-4S]$^{+}$ cluster (**Fig. 1e**, trace 1)[36]. The signal displayed significant relaxation broadening at temperatures above 30 K when recorded under non-saturating microwave power (**Extended Data Fig. 3a, b**). Consistent with this assignment, it disappeared in the A3-mutant, in which the three cysteines coordinating the radical SAM cluster have been substituted by alanines (**Fig. 1e**, trace 3). Iron-sulfur determination indicated that, in agreement with its UV-visible spectrum, the reconstituted wild-type EpeE contained 8.6 ±0.5 mol of Fe per mole of protein whereas the A3-mutant contained 4.8 mol ±0.13 of Fe per mole of protein (**Extended Data Fig. 3c**). This supports the presence of two and one [4Fe-4S] cluster in the wild-type and A3-mutant, respectively. Therefore, the absence of any other signal in the reduced wild-type or A3-mutant is consistent with the fact that the auxiliary cluster is in the EPR silent [4Fe-4S]$^{2+}$ redox state, most probably because of its very low redox potential as reported for other radical SAM enzymes[37,38]. The addition of SAM to the dithionite-reduced wild-type enzyme induced a substantial change in the resonance position and shape of the EPR spectrum. Notably, a signal from an *S* = ½ paramagnetic species having all *g*-values smaller than 2.00 (*i.e.* $g_{1,2,3}$ = (1.983, 1.871, 1.790)) was detected, as shown in the spectrum measured at 6 K under non-saturating conditions (**Fig. 1e**, trace 4 & **Extended Data Fig. 3a, b**). Absent from the **A3**-mutant (**Fig. 1e**, trace 6), this signal is assigned to a SAM-bound form of the radical SAM [4Fe-4S]$^{+}$ cluster. Radical SAM [4Fe-4S]$^{+}$ clusters having all *g*-values smaller than 2.0 have been reported for other enzymes[33,39,40] and generally associated with a cluster form in which SAM binds to the unique iron of cluster, an assignment further supported by HYSCORE measurements (**Extended Data Fig. 3d**).

Structure of EpeE in complex with a peptide substrate

Initial attempts to crystallize EpeE with its full-length substrate failed, as commonly encountered with RiPP-modifying enzymes. This recurrent failure likely results because of the intrinsically disordered nature of peptides and the fact that many RiPP-modifying enzymes have relaxed substrate specificity, essential to introduce post-translational modifications at distinct sites[41]. Indeed, EpeE like other radical SAM enzymes[15,42] introduces multiple post-translational modifications and must thus adapt to different peptide contexts. To circumvent this inherent difficulty, we designed a peptide library covering the leader and core sequence of the peptide substrate EpeX **1** (**Fig. 2a**). This RiPP-fragment library was assayed for activity and co-crystallization with EpeE. All peptides containing the core sequence (peptides **4**-**7**) proved to be substrates as shown by labeling experiments performed in deuterated buffer (**Extended Data Fig. 4, 5 and Supplementary Tables 1-8**)[9,15,43]. LC-MS/MS analysis notably confirmed that ^{2}H-atom incorporation occurred exclusively at the expected epimerization sites. Of note, with peptides **4** and **7**, we monitored significant uncoupling between SAM cleavage and epimerization activity, as revealed by 5'-dA isotopic enrichment (**Extended Data Fig. 4a, d**). In contrast, with peptides **5** and **6**, no solvent ^{2}H-atom was incorporated into 5'-dA, supporting a strict coupling with these substrates (**Extended Data Fig. 4b, c** & **Extended Data Fig. 5**).

Remarkably, EpeE co-crystallization assays under anaerobic conditions with SAH and the RiPP-fragment library, led to a high-resolution structure (2.39 Å) of EpeE in complex with peptide **5** (**Fig. 2a & b**). Crystal form in space group $P2_12_12_1$ was identical to the one obtained

when crystallizing the substrate-free enzyme, with an asymmetric unit consisting of a homodimer (**Extended Data Table 1**). Only subtle changes mainly located in the T-SPASM domain could be measured between the free- and bound-substrate structures (r.m.s.d of 0.78 Å, **Extended Data Fig. 6**). In addition, a strong electron density for the peptide **5** was observed for 7 out of 11 residues (**Extended Data Fig. 7a**). The peptide fits in the open cavity located at the bottom of the partial TIM barrel and binds between the β1-β5 of the radical SAM domain and the beginning of the T-SPASM domain (**Fig. 2b**). Peptide **5** is coordinated by a complex network of inter- and intra-molecular interactions folding partially the peptide into a 3_{10}-helix (**Extended Data Fig. 7b**). The residue target of the modification I44 is in the vicinity (3.6 Å) of the aromatic rings of F23 and F228 (**Fig. 2c**). Interestingly C223, which we proposed as the H-atom donor of the reaction[9], is part of the hydrophobic pocket around I44 and provides key interactions with I44 including a polar contact *via* its backbone oxygen and hydrophobic interactions. I44 is also stabilized through its backbone oxygen by hydrogen bonding with the sidechain oxygen of T57 (**Fig. 2c**). Further stabilization of the substrate is provided by π-π stacking between W43 and the aromatic ring of F175 (EpeE) (π-π centroids 4.6-5.4 Å). Finally, polar interactions with the adenine moiety of SAH (3.28 Å) and hydrophobic contacts with I178 and P225 (3.59 Å) are also involved in stabilizing I44 through W43 (**Fig. 2c**). The importance of W43 in peptide stabilization is consistent with the fact that the two epimerization sites (I44 and V36), despite lacking sequence homology, are preceded by an aromatic residue. Hence, EpeE appears to recognize a hydrophobic motif for epimerization installation. Further interactions between EpeE and its substrate involve salt bridges between the sidechain of D210 and the sidechains of two substrates residues, R42 and N41, this latter having also a direct interaction with G208 (**Fig. 2c**). The radical SAM domain through S55 and T57 side chains also contributes to peptide stabilization mainly through polar contacts, while T113 and L84 interact with L45 from the peptide through water contacts. Similarly, N147 (β5) coordinates a water molecule that makes polar contacts with three residues (T43, L45 and R42) from peptide **5** (**Fig. 2c**). Hence, the structure of the complex revealed that the substrate not only interacts with the two protein domains but also with the SAH cofactor. It also surprisingly showed that the substrate residues preceding I44 adopt a 3_{10}-helix secondary structure.

Cys223 as a critical H-atom donor

In the enzyme-substrate complex, the distance between the targeted substrate residue I44 C_α-atom and the C5'-atom of SAM (3.8 Å) is perfectly suited for direct H-atom abstraction from the substrate. Remarkably, on the opposite side of I44, we found C223 (S_{C223}-$C_{\alpha\text{-}I44}$-$C5'_{SAH}$ angle: 152°) with a sulfur (C223) to C_α-atom (I44) distance of 6.3 Å **(Fig. 2d**). Although this distance is too large for direct interaction between C223 and the transient peptide carbon-centered radical formed during catalysis, this distance is likely to shorten due to the loss of I44 stereochemistry. In addition, the structure of the D210A mutant (see below) has revealed that C223 can sample other conformations bringing the sulfhydryl group 2 Å closer to the radical SAM [4Fe-4S] cluster. Altogether, these data are in full agreement with the proposed role of C223 as the H-atom donor of the reaction.

Crystallographic snapshots of an EpeE active-site mutant

Because of the critical role of C223 in the epimerization reaction, we reasoned that the C223A mutant could provide further stabilization to the transient peptide-protein complex. Structure of this mutant perfectly superimposed with the one of the wild-type enzyme (r.m.s.d. value of 0.2945 Å,) with the SAM cofactor in direct interaction with the radical SAM [4Fe-4S] cluster.

EPR analysis of this mutant (**Fig. 1e**, traces 2 & 5), in the absence or the presence of SAM, showed identical EPR signatures than the wild-type EpeE, supporting that the electronic structure of the radical SAM [4Fe-4S]$^{+}$ cluster is not affected.

Gratifyingly, we solved the structure of the C223A mutant at an atomic resolution with peptide **5** and peptide **6** (1.75 Å and 2.15 Å, respectively) in the presence of SAH. Interactions between peptide **5** and the C223A mutant were overall similar to the wild-type enzyme (r.m.s.d 0.22 Å) (**Figs. 3a and Extended Data Fig. 8**). However, we obtained electron density for two additional *N*-terminal amino acid residues located at the very entrance of the active site and forming an additional turn, pointing toward the exit of the active site (**Fig. 3a and Extended Data Fig. 8c**).

The peptide **6**-C223A mutant complex revealed the structure of the full *C*-terminal end of EpeX **1** (**Fig. 3b and Extended Data Fig. 8c**). This final peptide segment is stabilized along three β-sheets from the partial TIM barrel (from β3 to β5) and points toward the exit of the active site with the final peptide residue H49 making polar contacts with I144, S145 and D143. Interestingly, D143 and K171 from EpeE are stacking H49 (**Fig. 3b**), while in the complex with peptide **5** (lacking H49) and in the substrate-free structure, D143 and K171 are stabilized by a salt bridge in a distinct orientation (**Extended Data Fig. 8d, e**).

The overlapping sequences of peptides **5** and **6** perfectly superimposed, demonstrating the validity of our RiPP-fragment based approach (**Fig. 3c**). Notably, in both complexes, the relative location of I44 within the active site, remains the same. Unexpectedly, the presence of H49 provides further inter-chain interactions between the two enzyme subunits (**Extended Data Fig. 8d, e**). Within the homo-dimeric complex, peptide-peptide interactions are thus likely to significantly contribute to stabilize a productive positioning of the substrate. Exploiting these two atomic-resolution structures, we were able to model, based on the visible electron density, the structure of a peptide spanning 13 residues long (**Fig. 3d**). In this model, I44 is part of a folded peptide region as a 3_{10}-helix while the final GSGH motif has an extended conformation. Remarkably, hydrophobic side-chains are protruding (I44, W43) and alternating with charged residues (E40, R42), reminiscent of the structure of α-helical antimicrobial peptides[44].

Structural basis for RiPP epimerization

As shown, in all the peptide-enzyme complexes obtained, I44 is perfectly positioned for Cα H-atom abstraction (**Fig. 4a**) and formation of a carbon-centered radical. This transient reaction intermediate is likely to react with the sulfhydryl of C223, leading to epimerization of I44 and the formation of a thiyl radical. With the auxiliary cluster (AuxI) in the vicinity of C223, a consistent function would be as an electron shuttle to the thiyl radical. Only few radical SAM RiPP-modifying enzymes have been spectroscopically characterized[37,45,46] but for some of them, the auxiliary cluster (AuxI) proved to be a low-potential [4Fe-4S] cluster[37]. In addition, recent investigations have shown that substrate binding can tune the redox properties of the AuxI cluster, further supporting a role as an electron shuttle[46]. In EpeE, AuxI is likely to fulfill a similar function with two tyrosine residues (Y209 and Y2) located beneath the cluster and stabilized by main chain interactions, hydrogen bonds and π-π stacking, ideally positioned to serve as an electron conduit from the protein surface (**Fig. 4a**). In addition, we also identified in the immediate environment of C223, only one titratable residue: D210. This residue provides key electrostatic interactions to the substrate (**Figs. 2c, 3a** and **3b**) and is stabilized by a polar bond with T5 (**Extended Data Fig. 9a**).

To probe for the function of these residues, we generated several mutants by substituting the two tyrosines with phenylalanine residues (Y2F-Y209F mutant) and by replacing D210 with an

alanine residue (D210A mutant). The activity of these mutants was assayed using peptide **6** as substrate and a physiological reducing system (NADPH/flavodoxin/flavodoxin reductase). As shown, we obtained a tight coupling between SAM cleavage (5'-dA production) and peptide epimerization with the wild-type enzyme (**Fig. 4b**). In contrast, with the C223A mutant, epimerization was strongly impaired while SAM cleavage activity remained similar to the wild-type enzyme. Hence, with the C223A mutant, only the epimerization reaction is affected. The two other mutants Y2F-Y209F and D210A had similar activities compared to the wild-type EpeE (**Fig. 4b**). However, under *in vitro* conditions, the physiological roles of these amino acid residues might be difficult to evidence because of the excess of reductant and electrons present in the reaction mixtures.

The high-resolution structure of the D210A mutant in complex with SAH (1.95 Å) was similar to the wild-type enzyme (r.m.s.d. of 0.25 Å). However, it exhibited two major differences: first, C223 adopted a distinct orientation bringing the sulfhydryl group 2 Å closer toward the SAH cofactor. Second, we noted the presence on C223 of an additional electron density (**Extended Data Fig. 9b**). This extra electron density was modeled, after analysis of the $2F_o$-F_c map maximum intensity, as a second sulfhydryl group (**Extended Data Fig. 9b**). The presence of a persulfur on a reactive cysteine has been reported in several systems including cytochrome thiosulfate dehydrogenase[47] or the cysteine desulfurase NifS[48]. In the D210A mutant, the origin of this additional sulfur atom is unknown but it supports that C223 is a reactive residue. Careful analysis of all structures showed that this adduct and this sidechain orientation were only present in the D210A mutant, supporting that D210 plays an important role to stabilize C223. Finally, polar contacts between D210 and T5 sidechains are also reminiscent of the catalytic "acid-alcohol pair" found in cytochrome P450[49] and involved in proton transfer within the active site. Collectively, these data support that D210 interacts with C223 and could play an important role not only in substrate stabilization and positioning, but also for C223 reactivity.

Discussion

Despite major advances in our understanding of RiPP biosynthesis, core peptide recognition by RiPP enzyme active sites is largely unknown. These enzymes must often recognize multiple modification sites to generate their final products, supporting a relaxed substrate specificity. Recent studies have shown that RiPP-modifying enzymes including radical SAM enzymes, while catalyzing a vast array of chemical transformations[1,2], share conserved structural features such as an RRE to interact with the leader peptide[10] and ensure the fidelity of the post-translational modifications. However, this structural element is absent from many enzymes questioning the processes underpinning their specificity.

To address these fundamental questions, we have investigated the radical SAM epimerase EpeE[9] alone and in complex with several peptide substrates. Structural and EPR analyses demonstrate that EpeE contains two [4Fe-4S] clusters and has an unusual architecture. Its compact fold markedly differs from all known RiPP-modifying radical SAM enzymes by the notable absence of an RRE domain and of the α6 and α4a helices from the partial TIM barrel. In addition, EpeE possesses a unique *C*-terminal domain which shares the single [4Fe-4S] cluster of twitch-domains but with an overall fold reminiscent of the SPASM-domain, that we propose to call a T-SPASM domain (**Figs. 1 & 2**).

By generating a RiPP-fragment library, we were able to obtain high-resolution crystallographic snapshots of a RiPP-modifying radical SAM enzyme in a pre-catalytic state (**Figs. 2b, c and**

Extended Data Fig. 8) with its substrate properly located in the active site. Currently, only two structures of radical SAM enzymes catalyzing RiPP post-translational modifications have been solved in complex with peptide substrates[29,30]. Intriguingly, in SuiB, which catalyzes the formation of carbon-carbon bonds, the leader peptide was found in the partial TIM barrel instead of the RRE and no electron density was present for the core peptide. For CteB which catalyzes thioether bond formation, only the leader peptide sequence and the first three residues of the core region were visible in the co-crystallized structure[30].

In sharp contrast, the structures of EpeE and its C223A mutant in complex with different peptide substrates revealed that I44, the amino acid residue target of the modification, is in an ideal position for direct C_α H-atom abstraction by the 5'-dA radical (I44 C_α-atom-C5' distance of 3.8 Å). Structural analysis also revealed that a conserved cysteine residue (C223) is located beneath I44 to serve as an H-atom donor. By using a physiological reductant system, we demonstrated that while the SAM cleavage activity is not affected by mutation of C223, the second part of the reaction (*i.e.* H-atom transfer to the carbon-centered radical) is hampered leading to a strong uncoupling between SAM cleavage and peptide epimerization (**Fig. 4b**). Interestingly, while the distance in the peptide-enzyme complex is too long (6.3 Å, **Fig. 2d**) for a direct interaction between C223 and the C_α-atom of I44, structural analysis of the D210A mutant revealed that C223 can sample various conformations, bringing the sulfur atom closer to the I44 C_α-atom. Altogether, these results support that radical SAM peptide epimerases effectively use a cysteine residue as critical H-atom donor, a strategy likely common to all radical SAM epimerases[15,50,51].

Another advantage of our RiPP-fragment based approach was to gain structural information regarding RiPP structure during catalysis. Indeed, based on the structure of several peptide-enzyme complexes, we were able to model up to 13 substrate residues, starting from the residue after V36 up to the *C*-terminal end of EpeX. This model reveals that EpeX is partially folded as a 3_{10}-helix in the enzyme active site with protruding hydrophobic side-chains. Although 3_{10}-helices have been identified in other RiPPs, the core region is usually unstructured or with a U-turn shape in RiPP-enzyme complexes[52-55].

In sharp contrast to the known structures of (non-radical SAM) RiPP-modifying enzymes[52-55], only minor rearrangements occurred in EpeE upon substrate binding. Peptide-enzyme interactions are driven not only by residues from the radical SAM domain but also by residues from the T-SPASM domain and the SAM cofactor itself, forging a complex network of interactions that ensure substrate recognition in the absence of RRE. Interestingly, a similar strategy implying interactions between the substrate backbone with the protein domains and the SAM cofactor, has been recently reported for the B_{12}-dependent radical SAM enzyme Mmp10[56].

Another intriguing finding of this study is that with peptide **6,** not only the full *C*-terminal end of epipeptide could be accommodated in the EpeE dimer without steric clashes but unexpectedly, further stabilization was provided by the last residue. Indeed, H49, stacked between K171 and D143, directly interacts through inter-chain interactions with H49 from the second subunit (**Extended Data Fig. 8d, e**), supporting a physiological role for the dimer (**Fig. 5a**). To validate this model, we performed anaerobic SEC-SAXS analysis in order to determine the oligomerization state of EpeE in solution. SEC-SAXS analysis showed that anaerobically reconstituted EpeE in the presence of SAM behaved as a homogenous globular and folded protein (**Fig. 5b**) with a radius of gyration of 28.7 Å and an estimated molecular weight of 73-71 kDa. These experimental data are consistent with EpeE being exclusively a dimer in

solution and are in full agreement with our structural analysis. Additionally, surface interaction calculations using the PDBePISA server[57] also supported that the dimer is the most stable species (**Supplementary Tables 9-10**). This dimer provides an elegant structural rationale for the installation of the two epimerizations in epipeptides. Initially, two peptide molecules interact within the EpeE dimer, positioning I44 in the active site for direct attack by the 5'-dA radical. The presence of a hydrophobic residue before each targeted residue is also likely to provide key stabilization. Following H-atom abstraction, the amino acid configuration is lost (**Fig. 5c**) and the radical substrate intermediate is quenched by C223, which is ideally located on the opposite side of the targeted residue. Similar critical cysteine residues have been identified in all radical SAM epimerases investigated to date[15,50,51]. After configuration inversion, a transient thiyl radical is generated on C223. D210 which forms a pair with T5 and stabilizes C223, is the only residue that could serve to regenerate the thiyl radical using a proton-coupled electron transfer pathway. Following, the first epimerization event, the dimer progresses toward V36 which is already in the vicinity the active site (**Fig. 5a**). In support of this model, not only we have always crystallized peptides with I44 positioned for H-atom abstraction but also I44 was always the hotspot for epimerization (**Extended Data Fig. 4**), suggesting a *C*-to-*N* directionality in EpeE like in PoyD[15].

In conclusion, our study reports an unprecedented binding mode for a RiPP-modifying enzyme and expands the structural diversity of radical SAM enzymes catalyzing RiPP post-translational modifications. Unexpectedly, the EpeE structure reveals that inter-chain interactions could play a significant role for the sequential installation of epimerizations. Finally, this work illuminates how radical SAM enzymes catalyze peptide epimerization, a rare example of redox-neutral reaction, delineating novel reactivity in enzyme active sites.

Acknowledgments

This work was supported by the French National Research Agency (ANR grants: ANR-17-CE11-0014 to O.B.; ANR-20-CE44-0005 to O.B.). The authors are grateful to the EPR facilities available at the French EPR network (IR CNRS 3443, now INFRANALYTICS, FR2054) and the Aix-Marseille University EPR center. We acknowledge SOLEIL (Saint-Aubin, France) for provision of synchrotron radiation facilities and we would like to thank the PROXIMA-1 and SWING staff for assistance in using the beamline.

Author contributions

A.B. & O.B. research design and funding acquisition; X.K., I.P., L.M.G.C., C.D.F., A.G., S.G., G.G., .A.T., P.L., O.B. & A.B performed research; X.K., I.P., L.F. & C.B. protein production. X.K., I.P., L.M.G.C., C.D.F., A.G., S.G., G.G., .A.T., P.L., O.B. & A.B. analyzed data. O.B. & A.B. wrote the manuscript with contributions from co-authors.

Competing Interests Statement

The authors declare no competing interests.

Additional information

Extended data is available for this paper.

Figure legends

Fig. 1 - Epipeptide biosynthesis and overall structure of the EpeE radical SAM epimerase. a, Sequence of EpeX precursor with the leader (white circles) and the core peptide sequence (blue circles) indicated. After modification by EpeE, the mature epipeptide is produced with epimerization of V36 and I44 (in red). **b,** Epimerization reaction catalyzed by EpeE showing the C_α H-atom, target of the modification, in red. **c,** Overall structure of the EpeE homodimer in the asymmetric unit (left panel). Radical SAM domain (light blue, residues 1-175) and T-SPASM domain coordinating the auxiliary (AuxI) [4Fe-4S] cluster (teal, residues 206-317). **d**, Crystal structure of EpeE with bound SAH. The [4Fe-4S] and AuxI clusters are shown as balls and sticks (yellow and orange spheres) and SAH as sticks (green). The omit map (blue mesh) of SAH and [4Fe-4S] clusters are contoured at 3σ. AuxI: auxiliary cluster. **e,** EPR analysis of EpeE. X-band CW EPR spectra of dithionite-reduced reconstituted samples of EpeE WT (traces 1, 4), C223A mutant (traces 2, 5) and **A3**-mutant (traces 3, 6) and in the absence (traces 1-3) and presence (traces 4-6) of an excess of SAM. Experimental conditions: temperature, 15 K (traces 1-3) or 6 K (trace 4-6), microwave power, 0.1 mW, field modulation amplitude, 1 mT, microwave frequency, 9.48 GHz, number of accumulations, 8 (1-3), or 16 (4-6). Protein concentration, 320 µM (1, 4), 223 µM (2, 5), 380 µM (3, 6), SAM concentration, 1 mM.

Fig. 2 - Structure of EpeE in interaction with a peptide substrate and SAH cofactor. a, Sequences of the peptide substrates assayed: EpeX (peptide **1**) and the RiPP-fragments: peptides **2**, **3**, **4**, **5**, **6** & **7**. The leader peptide is shown in white circles and the core peptide is indicated by blue circles. The two residues, targets of the modification by EpeE (*i.e.* V36 and I44) are shown in red in blue circles. **b**, Overall structure of EpeE in complex with the peptide **5** (left panel). The bound peptide **5** (residues K_{39}ENRWIL$_{45}$) is depicted in pink sticks, SAH is shown in green and the two [4Fe-4S] clusters are in yellow and orange. APBS-derived surface electrostatics of EpeE reveals three distinct electrostatic potentials in the EpeE peptide binding pocket (right panel). Surface colored according to electrostatic potential with positively charged regions in blue and negatively charged regions in red. The bound peptide is shown in pink sticks. **c**, Coordination of the peptide **5** (pink sticks) by both EpeE domains. The binding pocket within 5 Å of the peptide consists of 6 hydrophobic residues (F23, F175, F228, L84, I85, I178), five polar uncharged residues (S55, T57, T83, T113, S224), and three charged residues (N9, N147, D210), in addition to C223, P176 and P225. SAH, the radical SAM [4Fe-4S] and AuxI clusters are shown as sticks. Amino acid residues in light blue belong to the radical SAM domain and the ones in teal are from the T-SPASM domain. **d**, Close-up of the EpeE active site showing SAH in green, the peptide **5** in pink, C223 in teal and the two [4Fe-4S] clusters in yellow and orange. The distances between the C5′ atom of SAH and the C_α atom of I44 from peptide **5** (3.8 Å) and between I44 and the sulfur-atom of C223 from EpeE (6.3 Å) are indicated by dashed lines.

Fig. 3 - Structures of C223A mutant in interaction with two peptide substrates and SAH cofactor. a, Close-up of EpeE **C223A** mutant active site showing protein residues from the radical SAM (in light blue) and the T-SPASM (in teal) domains in interaction with the peptide **5** (in pink). Dashed lines show polar contacts between peptide **5** and protein residues. SAH is depicted in green sticks and both [4Fe-4S] clusters are shown in yellow and orange spheres. **b,** Close-up of EpeE **C223A** mutant active site showing protein residues from the radical SAM (in light blue) and the T-SPASM (in teal) domains in interactions with the peptide **6** (in light

green). Dashed lines show polar contacts between peptide **6** and protein residues. SAH is depicted in green sticks and both [4Fe-4S] clusters in yellow and orange spheres. The epipeptide C-terminal region points toward the exit of the active site with the last residue H49 interacting with residues 143-145. **c,** Superimposition of the structures of peptides **5** and **6** obtained from the respective complexes with the **C223A** EpeE mutant. **d**, Model of the 13 residues (KSKENRWILGSGH) identified in C223A EpeE mutant active site. The region that holds I44 is folded as a 3_{10}-helix while the *C*-terminal residues (GSGH) featured an extended conformation.

Fig. 4 – Amino acid network in the active site of the radical SAM enzyme EpeE. **a,** Close-up of EpeE active site with key residues highlighted. Distances are shown as dotted lines with values indicated in Å. **b,** Time-course analysis of epimerized peptide (open and closed squares) and 5′-dA (open and closed diamonds) production by EpeE and mutants (**C223A**, **D210A** & **Y2F**/**Y209F**) incubated with SAM and peptide **6** under anaerobic and reducing conditions with the flavodoxin/flavodoxin reductase/NADPH system. Experiments were performed in duplicate and analyzed by LC-MS.

Fig. 5 – Substrate interaction and proposed mechanism for EpeE. **a,** Model of epimerization catalyzed by EpeE on the EpeX peptide. In the EpeE dimer, two peptide molecules (EpeX) interact through inter- (H49) and intra-chain interactions with I44 positioned in the active site for an attack by the 5'-dA radical. After the first epimerization event, the dimer progresses toward V36, the second epimerized residue. **b**, SEC-SAXS analysis of EpeE in the presence of SAM (panel **1**) or SAM and peptide **6** (panel **2**). The UV visible signal at λ = 280 nm (blue) and SAXS intensity at zero angle (red) is superimposed with the computed Rg from SAXS data (open circles). SAXS curves of EpeE in the presence of SAM (panel **3**) and EpeE in the presence of SAM and peptide **6** (panel **4**). Fit curves using PepsiSAXS are indicated by a red trace and χ^2 value determined between the experimental data and the simulated model (*see* **Supplementary Table 10**). **c**, Proposed mechanism for EpeE. Following the reduction of the radical SAM cluster, the 5'-dA radical generated, abstracts the C_α H-atom of the target residue. The carbon-centered radical formed on the substrate reacts with C223, leading to configuration inversion of I44 and formation of a thiyl radical on C223. The AuxI [4Fe-4S] cluster, likely assisted by D210, is ideally positioned to regenerate C223 through a proton-coupled electron transfer pathway.

References

1. Montalban-Lopez, M. et al. New developments in RiPP discovery, enzymology and engineering. *Nat Prod Rep* **38**, 130-239 (2021).
2. Benjdia, A. & Berteau, O. Radical SAM Enzymes and Ribosomally-Synthesized and Post-translationally Modified Peptides: A Growing Importance in the Microbiomes. *Front Chem* **9**, 678068 (2021).
3. Benjdia, A. & Berteau, O. Sulfatases and radical SAM enzymes: emerging themes in glycosaminoglycan metabolism and the human microbiota. *Biochem. Soc. Trans.* **44**, 109-15 (2016).
4. Balty, C. et al. Ruminococcin C, an anti-clostridial sactipeptide produced by a prominent member of the human microbiota Ruminococcus gnavus. *J Biol Chem* (2019).
5. Balty, C. et al. Biosynthesis of the sactipeptide Ruminococcin C by the human microbiome: Mechanistic insights into thioether bond formation by radical SAM enzymes. *J Biol Chem* **295**, 16665-16677 (2020).
6. Balskus, E.P. The Human Microbiome. *ACS Infect. Dis.* **4**, 1-2 (2018).
7. Donia, M.S. et al. A systematic analysis of biosynthetic gene clusters in the human microbiome reveals a common family of antibiotics. *Cell* **158**, 1402-14 (2014).
8. Benjdia, A., Balty, C. & Berteau, O. Radical SAM Enzymes in the Biosynthesis of Ribosomally Synthesized and Post-translationally Modified Peptides (RiPPs). *Front. Chem.* **5**, 87 (2017).
9. Benjdia, A., Guillot, A., Ruffié, P., Leprince, J. & Berteau, O. Post-translational modification of ribosomally synthesized peptides by a radical SAM epimerase in Bacillus subtilis. *Nat Chem* **9**, 698-707 (2017).
10. Burkhart, B.J., Hudson, G.A., Dunbar, K.L. & Mitchell, D.A. A prevalent peptide-binding domain guides ribosomal natural product biosynthesis. *Nat Chem Biol* **11**, 564-70 (2015).
11. Heck, S.D. et al. Posttranslational amino acid epimerization: enzyme-catalyzed isomerization of amino acid residues in peptide chains. *Proc Natl Acad Sci U S A* **93**, 4036-9 (1996).
12. Huo, L. & van der Donk, W.A. Discovery and Characterization of Bicereucin, an Unusual d-Amino Acid-Containing Mixed Two-Component Lantibiotic. *J Am Chem Soc* **138**, 5254-7 (2016).
13. Lohans, C.T., Li, J.L. & Vederas, J.C. Structure and biosynthesis of carnolysin, a homologue of enterococcal cytolysin with D-amino acids. *J Am Chem Soc* **136**, 13150-3 (2014).
14. Freeman, M.F. et al. Metagenome mining reveals polytheonamides as posttranslationally modified ribosomal peptides. *Science* **338**, 387-90 (2012).
15. Parent, A. et al. Mechanistic Investigations of PoyD, a Radical S-Adenosyl-l-methionine Enzyme Catalyzing Iterative and Directional Epimerizations in Polytheonamide A Biosynthesis. *J Am Chem Soc* **140**, 2469-2477 (2018).
16. Butcher, B.G., Lin, Y.P. & Helmann, J.D. The yydFGHIJ operon of Bacillus subtilis encodes a peptide that induces the LiaRS two-component system. *J Bacteriol* **189**, 8616-25 (2007).
17. Popp, P.F. et al. The Epipeptide Biosynthesis Locus epeXEPAB Is Widely Distributed in Firmicutes and Triggers Intrinsic Cell Envelope Stress. *Microb Physiol*, 1-12 (2021).
18. Popp, P.F., Benjdia, A., Strahl, H., Berteau, O. & Mascher, T. The Epipeptide YydF Intrinsically Triggers the Cell Envelope Stress Response of Bacillus subtilis and Causes Severe Membrane Perturbations. *Front Microbiol* **11**, 151 (2020).
19. Radeck, J. et al. Anatomy of the bacitracin resistance network in Bacillus subtilis. *Mol Microbiol* **100**, 607-20 (2016).
20. Benjdia, A. et al. The thiostrepton A tryptophan methyltransferase TsrM catalyses a cob(II)alamin-dependent methyl transfer reaction. *Nat. Commun.* **6**, 8377 (2015).
21. Pierre, S. et al. Thiostrepton tryptophan methyltransferase expands the chemistry of radical SAM enzymes. *Nat. Chem. Biol.* **8**, 957-9 (2012).
22. Parent, A. et al. The B12-radical SAM enzyme PoyC catalyzes valine C-beta-methylation during polytheonamide biosynthesis. *J. Am. Chem. Soc.* **138**, 15515-15518 (2016).
23. Freeman, M.F., Helf, M.J., Bhushan, A., Morinaka, B.I. & Piel, J. Seven enzymes create extraordinary molecular complexity in an uncultivated bacterium. *Nat Chem* **9**, 387-395 (2017).

24. Benjdia, A. et al. Insights into the catalysis of a lysine-tryptophan bond in bacterial peptides by a SPASM domain radical S-adenosylmethionine (SAM) peptide cyclase. *J. Biol. Chem.* **292**, 10835-10844 (2017).
25. Balty, C. et al. Ruminococcin C, an anti-clostridial sactipeptide produced by a prominent member of the human microbiota Ruminococcus gnavus. *J Biol Chem* **294**, 14512-14525 (2019).
26. Benjdia, A. et al. Insights into the catalysis of a lysine-tryptophan bond in bacterial peptides by a SPASM domain radical S-adenosylmethionine (SAM) peptide cyclase. *J Biol Chem* **292**, 10835-10844 (2017).
27. Dowling, D.P. et al. Radical SAM enzyme QueE defines a new minimal core fold and metal-dependent mechanism. *Nat Chem Biol* **10**, 106-12 (2014).
28. Goldman, P.J., Grove, T.L., Booker, S.J. & Drennan, C.L. X-ray analysis of butirosin biosynthetic enzyme BtrN redefines structural motifs for AdoMet radical chemistry. *Proc Natl Acad Sci U S A* **110**, 15949-54 (2013).
29. Davis, K.M. et al. Structures of the peptide-modifying radical SAM enzyme SuiB elucidate the basis of substrate recognition. *Proc Natl Acad Sci U S A* (2017).
30. Grove, T.L. et al. Structural Insights into Thioether Bond Formation in the Biosynthesis of Sactipeptides. *J. Am. Chem. Soc.* **139**, 11734-11744 (2017).
31. Vey, J.L. & Drennan, C.L. Structural insights into radical generation by the radical SAM superfamily. *Chem Rev* **111**, 2487-506 (2011).
32. Haft, D.H. & Basu, M.K. Biological systems discovery in silico: radical S-adenosylmethionine protein families and their target peptides for posttranslational modification. *J. Bacteriol.* **193**, 2745-55 (2011).
33. Benjdia, A. et al. Anaerobic sulfatase-maturating enzyme--a mechanistic link with glycyl radical-activating enzymes? *FEBS J* **277**, 1906-20 (2010).
34. Grell, T.A.J. et al. Structural and spectroscopic analyses of the sporulation killing factor biosynthetic enzyme SkfB, a bacterial AdoMet radical sactisynthase. *J. Biol. Chem.* (2018).
35. Grell, T.A., Goldman, P.J. & Drennan, C.L. SPASM and twitch domains in S-adenosylmethionine (SAM) radical enzymes. *J. Biol. Chem.* **290**, 3964-71 (2015).
36. Broderick, J.B., Duffus, B.R., Duschene, K.S. & Shepard, E.M. Radical S-adenosylmethionine enzymes. *Chem Rev* **114**, 4229-317 (2014).
37. Tao, L., Zhu, W., Klinman, J.P. & Britt, R.D. Electron Paramagnetic Resonance Spectroscopic Identification of the Fe-S Clusters in the SPASM Domain-Containing Radical SAM Enzyme PqqE. *Biochemistry* **58**, 5173-5187 (2019).
38. Zhu, W. et al. Structural Properties and Catalytic Implications of the SPASM Domain Iron-Sulfur Clusters in Methylorubrum extorquens PqqE. *J Am Chem Soc* **142**, 12620-12634 (2020).
39. Yokoyama, K., Ohmori, D., Kudo, F. & Eguchi, T. Mechanistic study on the reaction of a radical SAM dehydrogenase BtrN by electron paramagnetic resonance spectroscopy. *Biochemistry* **47**, 8950-60 (2008).
40. Blaszczyk, A.J. et al. Spectroscopic and Electrochemical Characterization of the Iron-Sulfur and Cobalamin Cofactors of TsrM, an Unusual Radical S-Adenosylmethionine Methylase. *J Am Chem Soc* **138**, 3416-26 (2016).
41. Weerasinghe, N.W., Habibi, Y., Uggowitzer, K.A. & Thibodeaux, C.J. Exploring the Conformational Landscape of a Lanthipeptide Synthetase Using Native Mass Spectrometry. *Biochemistry* **60**, 1506-1519 (2021).
42. Benjdia, A. et al. Thioether bond formation by SPASM domain radical SAM enzymes: Calpha H-atom abstraction in subtilosin A biosynthesis. *Chem Commun (Camb)* **52**, 6249-6252 (2016).
43. Morinaka, B.I. et al. Radical S-adenosyl methionine epimerases: regioselective introduction of diverse D-amino acid patterns into peptide natural products. *Angew Chem Int Ed Engl* **53**, 8503-7 (2014).
44. Dathe, M. & Wieprecht, T. Structural features of helical antimicrobial peptides: their potential to modulate activity on model membranes and biological cells. *Biochim Biophys Acta* **1462**, 71-87 (1999).

45. Ayikpoe, R. et al. Spectroscopic and Electrochemical Characterization of the Mycofactocin Biosynthetic Protein, MftC, Provides Insight into Its Redox Flipping Mechanism. *Biochemistry* **58**, 940-950 (2019).
46. Balo, A.R. et al. Trapping a cross-linked lysine-tryptophan radical in the catalytic cycle of the radical SAM enzyme SuiB. *Proc Natl Acad Sci U S A* **118**(2021).
47. Brito, J.A., Denkmann, K., Pereira, I.A., Archer, M. & Dahl, C. Thiosulfate dehydrogenase (TsdA) from Allochromatium vinosum: structural and functional insights into thiosulfate oxidation. *J Biol Chem* **290**, 9222-38 (2015).
48. Nakamura, R., Hikita, M., Ogawa, S., Takahashi, Y. & Fujishiro, T. Snapshots of PLP-substrate and PLP-product external aldimines as intermediates in two types of cysteine desulfurase enzymes. *FEBS J* **287**, 1138-1154 (2020).
49. Denisov, I.G., Makris, T.M., Sligar, S.G. & Schlichting, I. Structure and chemistry of cytochrome P450. *Chem Rev* **105**, 2253-77 (2005).
50. Kudo, F., Hoshi, S., Kawashima, T., Kamachi, T. & Eguchi, T. Characterization of a radical S-adenosyl-L-methionine epimerase, NeoN, in the last step of neomycin B biosynthesis. *J Am Chem Soc* **136**, 13909-15 (2014).
51. Besandre, R.A. et al. HygY Is a Twitch Radical SAM Epimerase with Latent Dehydrogenase Activity Revealed upon Mutation of a Single Cysteine Residue. *J Am Chem Soc* **143**, 15152-15158 (2021).
52. Dong, S.H., Liu, A., Mahanta, N., Mitchell, D.A. & Nair, S.K. Mechanistic Basis for Ribosomal Peptide Backbone Modifications. *ACS Cent Sci* **5**, 842-851 (2019).
53. Zhao, G. et al. Structural Basis for a Dual Function ATP Grasp Ligase That Installs Single and Bicyclic omega-Ester Macrocycles in a New Multicore RiPP Natural Product. *J Am Chem Soc* **143**, 8056-8068 (2021).
54. Song, I. et al. Molecular mechanism underlying substrate recognition of the peptide macrocyclase PsnB. *Nat Chem Biol* **17**, 1123-1131 (2021).
55. Miller, F.S. et al. Conformational rearrangements enable iterative backbone N-methylation in RiPP biosynthesis. *Nat Commun* **12**, 5355 (2021).
56. Fyfe, C.D. et al. Crystallographic snapshots of a B12-dependent radical SAM methyltransferase. *Nature* **602**, 336-342 (2022).
57. Krissinel, E. & Henrick, K. Inference of macromolecular assemblies from crystalline state. *J Mol Biol* **372**, 774-97 (2007).

Methods

Cloning of EpeE D210A and Y2F-Y209F mutants

The EpeE tyrosine mutants were obtained by site-directed mutagenesis with the plasmid pET28-Strep-TEV-EpeE used as DNA template. To generate the Y2F-Y209F mutant the following primers were used: 5'-CAT ATG TTC AAC AAA ACC GTG AGC-3' ; 5'-TCC GGG TTT CGA TAT TGT GTA TCA TC-3' ; 5'-ACA ATA TCG AAA CCC GGA CAA TGC AG-3'. PCR reactions typically contained 1 µM of each primer, 250 µM of each dNTP, 1 µl of High Fidelity Polymerase (Thermo), ~50 ng DNA template and performed using the following PCR cycling parameters: 1 cycle at 95°C for 2 min followed by 36 cycles of 95°C for 30 sec (denaturation), 55-60°C for 30 sec (hybridation), 72°C for 90 s (extension) and 1 cycle at 72°C for 10 min. PCR products were purified on 1-2% agarose gel, digested with NdeI and XhoI (NEB), purified and ligated into NdeI/XhoI digested pET28-Strep-TEV plasmid. The D210A mutant gene was synthesis by GeneCust and ligated in plasmid pET28. The ligation products were transformed into chemically competent E. coli BL21 (DE3) star strain. Clones were selected on LB agar plate containing 50 $\mu g.mL^{-1}$ kanamycine. One clone was selected after we checked the sequence of the targeted gene by DNA sequencing.

Protein purification

The constructs of wild-type and C223A mutant streptavidin-tagged EpeE were the same as previously published[9]. All recombinant proteins were overexpressed and purified as follows. Typically, 9 L of *E. coli* BL21 cells transformed with pET28 plasmid containing the construct were grown in Luria-Broth (LB) media at 37°C with 50 µg/mL Kanamycin, and protein expression induced at Abs_{600nm} ~ 0.6 with 700 µM IPTG. Overexpression was conducted overnight and cells resuspended in Buffer A (500 mM NaCl, 50 mM TrisHCl, pH 8.0) containing 0.5% Triton X-100, protease inhibitors and sonicated for 4 min on ice. Cell debris were pelleted by ultracentrifugation at 45,000 g (Beckman coulter) before loading supernatant on Streptactin resin (IBA) equilibrated in buffer A. After washing in buffer A, the recombinant protein was eluted with buffer A supplemented by 3 mM desthiobiotin. Protein was aliquoted, flash frozen in liquid N_2 and stored at -80°C. Concentration was measured by absorbance at 280 (using ProtParam calculated ε and molecular weights) and purity assessed by SDS-PAGE on 12% gels and PageBlue staining.

Iron sulfur clusters reconstitution

In vitro reconstitution of the EpeE [4Fe-4S] clusters was achieved in presence of 3 mM DTT by addition of 8 molar excess of $(NH_4)_2Fe(SO_4)_2$ and Na_2S. After incubation under anaerobic atmosphere, excess of unbound iron and sulfur was removed onto a desalting column against buffer A with 3 mM DTT. Reconstitution of the protein was verified by recording UV-visible spectra (250-700 nm).

Peptide synthesis

The EpeX peptide **1** and RiPP-fragments peptide **2** (KKEITNNETVKNLEFKGLLDESQKLAKVNDL), peptide **3** (KNLEFKGLLDESQKLAKVNDL), peptide **4** (WYF**V**KSKEN), peptide **5** (F**V**KSKENRW**I**L), peptide **6** (KENRW**I**LGSGH), peptide **7** (NRW**I**LGSGH) were synthesized by solid-phase synthesis (ProteoGenix, France). In bold, residues targeted by EpeE.

EPR analysis

EPR samples were prepared immediately after reconstitution of the iron-sulfur clusters in the glove box. Reduction was achieved in 5 minutes by the addition of 3 mM sodium dithionite. Samples in the presence of SAM were prepared by addition of 3-5 fold stoichiometric excess of SAM. Samples were then frozen in liquid isopentane in the glove box and then maintained in liquid nitrogen until EPR measurements were performed. EPR spectra were recorded on a Bruker ElexSys-500 X-band spectrometer equipped with a standard rectangular cavity (ST4102) fitted to an Oxford Instruments liquid helium cryostat (ESR900) and temperature control system. The spectrometer settings were as follows: microwave frequency, 9.48 GHz, conversion time of 80 ms, modulation amplitude of 1 mT, and modulation frequency of 100 kHz. Other settings are given in the corresponding figure captions.

HYSCORE experiments were measured at 6 K using a Bruker EleXsys E580 spectrometer equipped with an ER4118X-MD5 dielectric resonator and an Oxford Instruments CF 935 cryostat. This four-pulse experiment ($\pi/2$-τ-$\pi/2$-t_1-π-t_2-$\pi/2$-τ-echo) was employed with an appropriate 8 step phase-cycling scheme to eliminate unwanted features from the experimental electron spin echo envelopes. The intensity of the echo after the fourth pulse was integrated over 32 ns with varied t_2 and t_1 and constant τ. The length of a $\pi/2$ pulse was 12 ns and of a π pulse 24 ns. A τ value of 132 ns and a shot repetition rate of 1 kHz were used. HYSCORE data were collected in the form of 2D time-domain patterns containing 256 × 256 points with steps of 16 ns. Spectra were recorded at the magnetic field value corresponding to the maximum absorption of the $[4Fe\text{-}4S]^{1+}$ signal in the absence of SAM (corresponding to $g = 1.929$). HYSCORE spectra were processed using Bruker's Xepr software. Relaxation decays were subtracted (fitting by 3rd order polynomial functions) followed by zero-filling to 1024 points and tapering with a Hamming window, before 2D Fourier transformation which finally gives the spectrum in frequency domain. Processed data were then imported into Matlab (The MathWorks Inc., Natick, MA) for plotting. HYSCORE spectra are shown in absolute value mode and are presented as contour plots.

Enzyme assay

The activity of EpeE towards the synthetic peptides was assayed in deuterated buffer (150 mM KCl, 25 mM TrisDCl, pH 8.0, DTT 3 mM); all compounds were dissolved in D_2O and the reconstituted protein was buffer exchanged against deuterated buffer. EpeE (235 µM) was incubated with 3 mM DTT, 3 mM SAM and 2.25 mM peptide. The reactions were initiated by addition of 3 mM sodium dithionite.

For the kinetic experiments, the EpeE WT, C223A, D210A and Y2F-Y209F mutants (100µM) were incubated with 1 mM SAM, 500µM peptide **6** and reactions were initiated with the addition of flavodoxin/flavodoxin reductase and 2.7 mM NADPH. All reactions were performed at 25°C and 15 µL aliquots sampled overtime for LC-MS/MS analysis.

Liquid chromatography–mass spectrometry/mass spectrometry analysis

LC-MS/MS analysis were achieved using a Q-Exactive Focus mass spectrometer (ThermoFisher Scientific) with the HESI2 electrospray ion source associated to a Vanquish Flex LC system (Thermo Fisher Scientific). Molecule separation was performed on a Zorbax Eclipse Plus C18 column (2.1X50mm, 1.8µm, RRHT, Agilent). Samples were dilute one hundred time before injection with TFA 0.1% or in acetonitrile 50%, to discard the protein by precipitation. Peptides **4**, **5**, **6** or **7** were eluted on the reverse phase column by an acetonitrile gradient with formic acid 0.1% as ion pairing agent and detected by mass spectrometry in positive mode. The doubly charged ions corresponding to the peptides **4**, **5**, **6**, **7** were selected for HCD fragmentation step at 35 % or 20 % of NCE. For detection and quantitation of the epimerized peptide **5** by mass spectrometry, the samples were hydrolyzed using trypsin Promega (V5111) to produce the peptide fragment WILGSGH and extract the corresponding MS signal of the doubly charge ion (385.21^{2+}). This method enables us to quantify the epimerized and unmodified peptides. Unmodified peptide fragment eluted at 13.7 min and the epimerized fragment at 18.2 min from the column. The 5′-dA produced during *in vitro* reactions with EpeE (wild-type and D210A, C223A and Y2F-Y209F mutants) was quantified in the sample by mass spectrometry using a direct standard curve of 5′-dA.

Crystallization of EpeE, EpeE C223A, EpeE D210A mutants and complexes with peptides 5 and 6

For crystallization purposes, the freshly reconstituted protein was further purified by size exclusion on a Superdex-200 10/300 GL Increase column (Äkta system, GE Healthcare) to achieve homogeneity in the protein preparation. Protein was then typically concentrated to 20 mg/mL before setting up crystallization experiments. Crystals were obtained by using the sitting drop vapor diffusion technique at 21°C under anaerobic atmosphere. After several rounds of optimization, brown rod shaped single crystals were obtained in 3 % Ethylene Glycol, 9.6 % PEG 8,000, 0.1 M HEPES pH 7.5, with a 2:1 protein:mother liquor ratio, and were used for anomalous data collection (**EpeE phasing dataset, Extended Table 1**). EpeE wild-type crystals (**EpeE WT**, **Extended Table 1**) appeared within 24 h by using hanging drop diffusion and a 1:1 mixing of protein (7.5 mg ml^{-1} with 0.5 mM SAH) and precipitant solution (0.1 M Tris-HCl pH 8.5, 17.5 % polyethylene glycol (PEG) 1,000). EpeE D210A mutant crystals (**EpeE D210A**, **Extended Table 1**) were grown in same conditions as EpeE WT in presence of SAH. EpeE C223A mutant crystals (**EpeE C223A**, **Extended Table 1**) were grown in 2:1 drops mixing protein (10 mg ml^{-1} with 1 mM SAM) and precipitant solution. The crystals of complexes from EpeE wild-type (**EpeE WT peptide 5**, **Extended Table 1**) and EpeE C223A mutant (**EpeE C223A peptide 5**, **EpeE C223A peptide 6**, **Extended Table 1**) were obtained mixing precipitants (0.1 M Tris-HCl pH 8.5, 14-20% PEG 1,000) with protein, SAH (0.5 mM) and peptide (5 mM). All crystals were typically obtained within 24 hours under anaerobic atmosphere and flash cooled in liquid N_2 under anaerobic conditions.

Crystallographic structure determinations

X-ray diffraction data were recorded on PROXIMA-1 beamline at Synchrotron SOLEIL [58], equipped with a Pilatus-6M hybrid pixel detector [59] and a three-axis SmarGon goniometer. An X-ray energy of 7.14 keV was chosen for the single anomalous phasing experiments, for which two sets of images were recorded at two different Chi angles to favor obtaining a more complete merged data at 2.99 Å resolution. The X-ray energy was 12.67 keV for subsequent data collection. For the experimental phasing measurements, the X-ray energy was attenuated to 5% of the beam intensity, providing with a flux of 1.0×10^{10} photons.s^{-1} at the sample position; the more standard data at 12.67 keV were recorded with 20% of the beam intensity. Phasing and data analysis and processing was performed using SHARP/AutoSHARP (SHARP 2.8.12 and Sushi 3.10.11), and the CCP4 suite (7.1.016). Data were processed with *XDS* 2022/01/10[60] through the *xdsme* scripting package[61]. The (hkl) and (-h-k-l) reflections were treated separately in all steps, including scaling and merging. Data sets were scaled with *XSCALE* 2022/01/10[60], converted to MTZ format with *POINTLESS* 1.12.13[62] and merged with *AIMLESS* 0.7.8[63], as implemented within the *xdsme* automated procedure.

For the EpeE phasing dataset, structure-factor amplitudes were obtained with *TRUNCATE* 8.0.010[64]. The Matthews coefficient suggested that the crystal contained two monomers *per* asymmetric unit. Four iron cluster sites were located with *SHELXC/D* 2016/1[65], and their respective positions were refined with *SHELXE* 2019/1 (through *HKL2MAP*) [66] and Phaser 2.8[67]. Initial correct substructures were determined immediately with *SHELXD* 2013/2, with two well-separated clusters in the plot of CC_{all} versus CC_{weak}. The phase information was improved using the existing non-crystallographic symmetry (NCS) between the two molecules within the asymmetric unit. One helix surrounding the iron clusters was docked in the original electron density using *Coot* [68] to facilitate the calculation of the matrix. Given this matrix, *Phaser* unequivocally identified the rotation and translation parameters of two monomers and confirmed the space group $P2_12_12_1$. Side chains were placed by automated model building with *Buccaneer* 1.6.12/*REFMAC5* [69]. Missing residues, water molecules and ligands were fitted in the $2F_o$-F_c and F_o-F_c electron-density maps using *Coot*. For structure refinements of the subsequent models, phases were introduced from the original structure as a template coordinates (Phaser) and the structures were refined iteratively with *REFMAC5* or *BUSTER* (version 2.10.4)[70]. Manual building was performed with *Coot* (version 0.9.6.1.1). The structures were validated by *MolProbity* as implemented in phenix version 1.19.2-4158[71]. Data collection and refinement statistics are shown in **Extended Table 1**. All structural representations were generated with PyMOL v0.99 (DeLano Scientific LLC) or PyMOL v2.5 (Schrödinger, LLC).

SEC-SAXS data measurement

All the data was collected in SEC-SAXS mode with an in-line Superdex 200 Increase 5/150 GL column (GE Healthcare). Homogeneous reconstituted proteins were loaded on our anaerobic setup which was based on an HPLC system equilibrated with degassed buffer containing 1 mM DTT and an auto-sampler flushed by a continuous flux of N_2. The SAXS data was collected at the SWING beamline at the SOLEIL synchrotron, France, equipped with an Eiger 4M detector with a sample-to-

detector distance of 2 m[72]. The parameters used for SAXS data collection are given in **Supplementary Table 10**. More information is available in **Supplementary Table 10.**

Reporting summary

Further information on research design is available in the Nature Research Reporting Summary linked to this paper.

Data Availability

Atomic coordinates and structure factors for the reported crystal structures in this work have been deposited in the Protein Data Bank upon accession codes: 8AI1, 8AI2, 8AI3, 8AI4, 8AI5 & 8AI6. SAXS data have been deposited in the Small Angle Scattering Biological Data Bank upon accession codes SASDRS7, SASDRR7. The data for this study are available within the paper and its Supplementary Information. Source data are provided with this paper.

References

58. Coati, A. et al. Status of the crystallography beamlines at synchrotron SOLEIL⋆. *The European Physical Journal Plus* **132**(2017).
59. Kraft, P. et al. Performance of single-photon-counting PILATUS detector modules. *Journal of Synchrotron Radiation* **16**, 368-375 (2009).
60. Kabsch, W. *XDS*. *Acta Crystallographica Section D Biological Crystallography* **66**, 125-132 (2010).
61. Legrand, p. XDSME: XDS Made Easier. GitHub repository (2017).
62. Evans, P. Scaling and assessment of data quality. *Acta Crystallographica Section D Biological Crystallography* **62**, 72-82 (2006).
63. Evans, P.R. & Murshudov, G.N. How good are my data and what is the resolution? *Acta Crystallographica Section D Biological Crystallography* **69**, 1204-1214 (2013).
64. Winn, M.D. et al. Overview of the *CCP* 4 suite and current developments. *Acta Crystallographica Section D Biological Crystallography* **67**, 235-242 (2011).
65. Sheldrick, G.M. A short history of SHELX. *Acta Crystallogr A* **64**, 112-22 (2008).
66. Pape, T. & Schneider, T.R. *HKL2MAP* : a graphical user interface for macromolecular phasing with *SHELX* programs. *Journal of Applied Crystallography* **37**, 843-844 (2004).
67. McCoy, A.J. et al. *Phaser* crystallographic software. *Journal of Applied Crystallography* **40**, 658-674 (2007).
68. Emsley, P., Lohkamp, B., Scott, W.G. & Cowtan, K. Features and development of *Coot*. *Acta Crystallographica Section D Biological Crystallography* **66**, 486-501 (2010).
69. Murshudov, G.N. et al. *REFMAC* 5 for the refinement of macromolecular crystal structures. *Acta Crystallographica Section D Biological Crystallography* **67**, 355-367 (2011).
70. Smart, O.S. et al. Exploiting structure similarity in refinement: automated NCS and target-structure restraints in *BUSTER*. *Acta Crystallographica Section D Biological Crystallography* **68**, 368-380 (2012).
71. Chen, V.B. et al. *MolProbity* : all-atom structure validation for macromolecular crystallography. *Acta Crystallographica Section D Biological Crystallography* **66**, 12-21 (2010).
72. Thureau, A., Roblin, P. & Perez, J. BioSAXS on the SWING beamline at Synchrotron SOLEIL. *Journal of Applied Crystallography* **54**, 1698-1710 (2021).

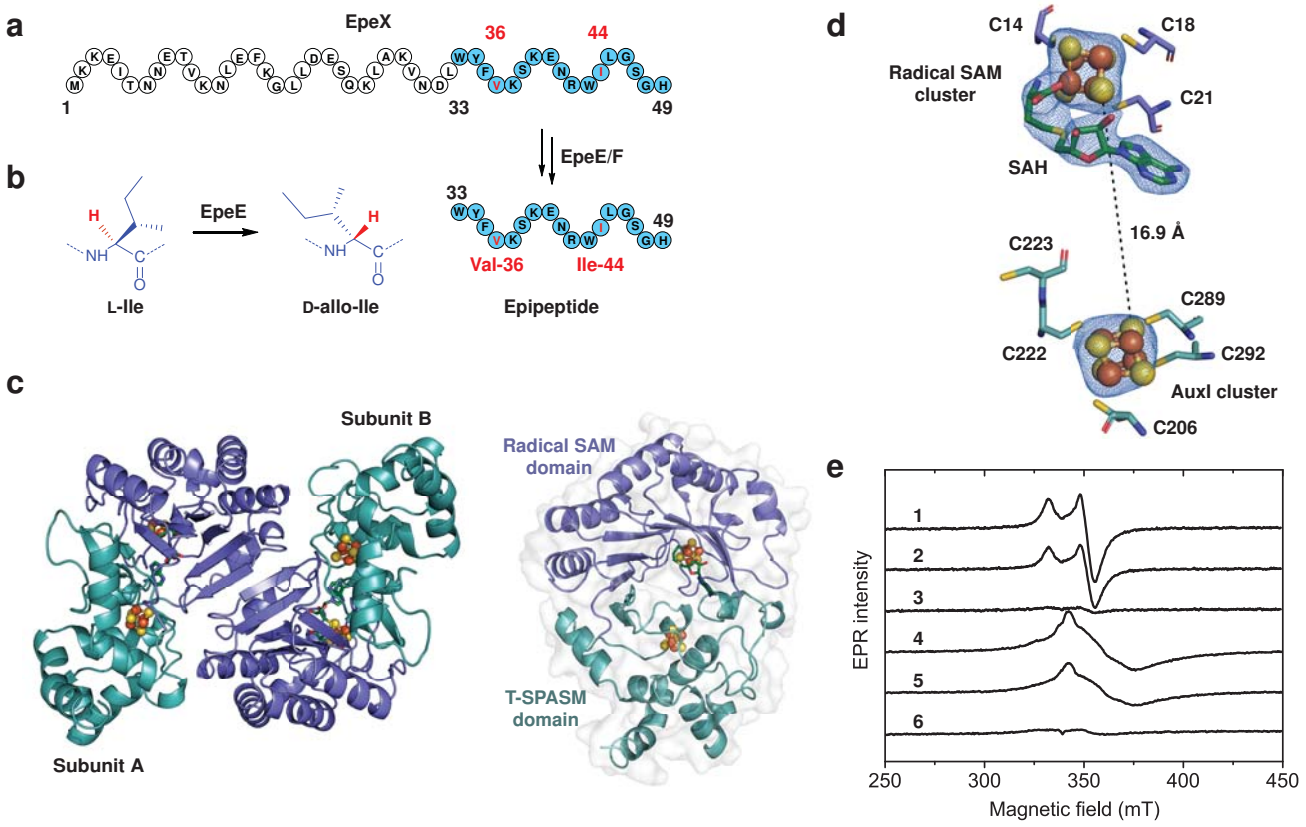
a
EpeX
36
44
1
33
49
b
EpeE
EpeE/F
L-Ile
D-allo-Ile
Epipeptide
Val-36
Ile-44
c
Subunit B
Subunit A
Radical SAM domain
T-SPASM domain
d
C14
C18
Radical SAM cluster
C21
SAH
16.9 Å
C223
C289
C222
C292
Auxl cluster
C206
e
EPR intensity
Magnetic field (mT)
250
300
350
400
450

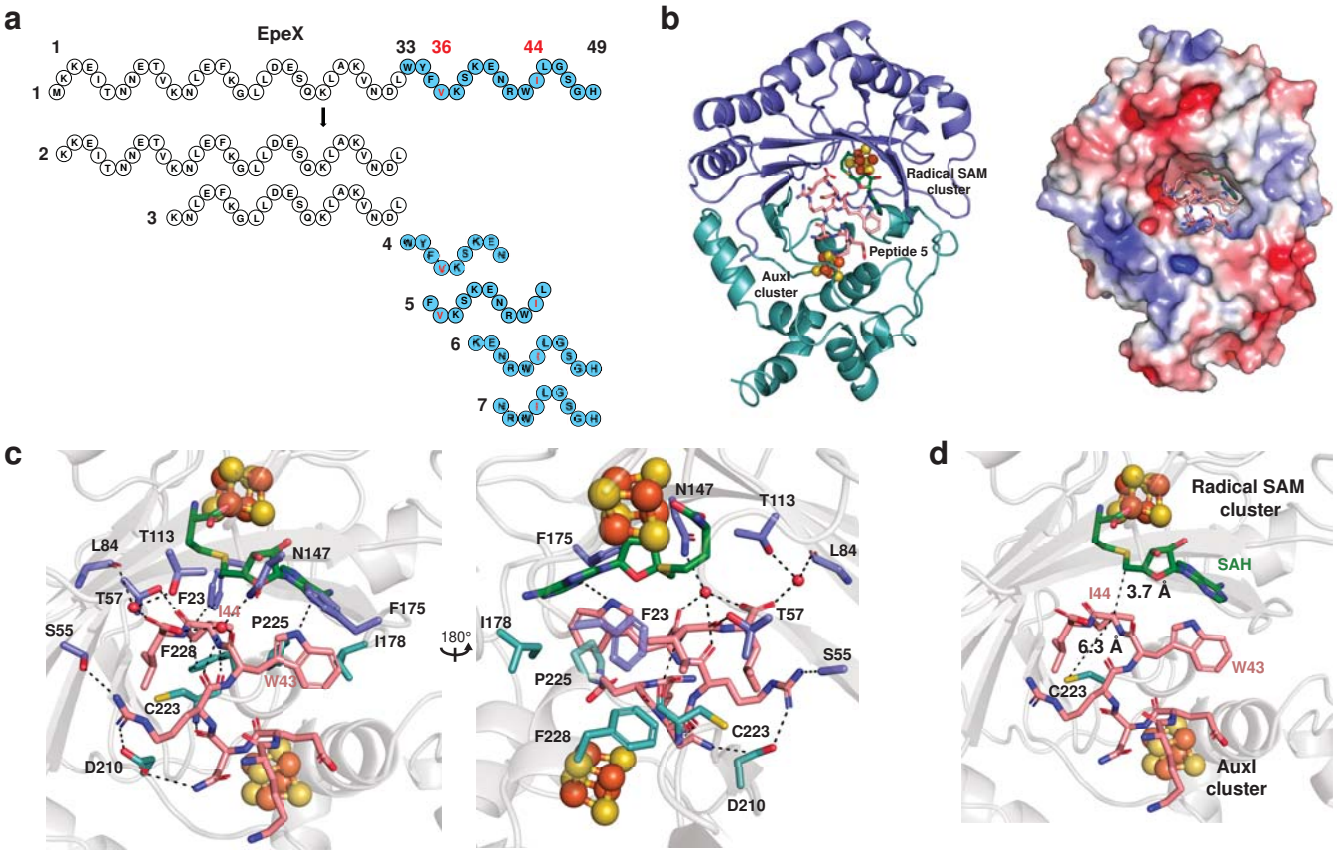
a
EpeX
1
33
36
44
49
1
2
3
4
5
6
7
b
Radical SAM cluster
Peptide 5
AuxI cluster
c
L84
T113
N147
T57
F23
I44
P225
F175
S55
F228
I178
W43
C223
D210
180°
N147
T113
F175
L84
F23
T57
I178
S55
P225
C223
F228
D210
d
Radical SAM cluster
SAH
I44
3.7 Å
6.3 Å
W43
C223
AuxI cluster

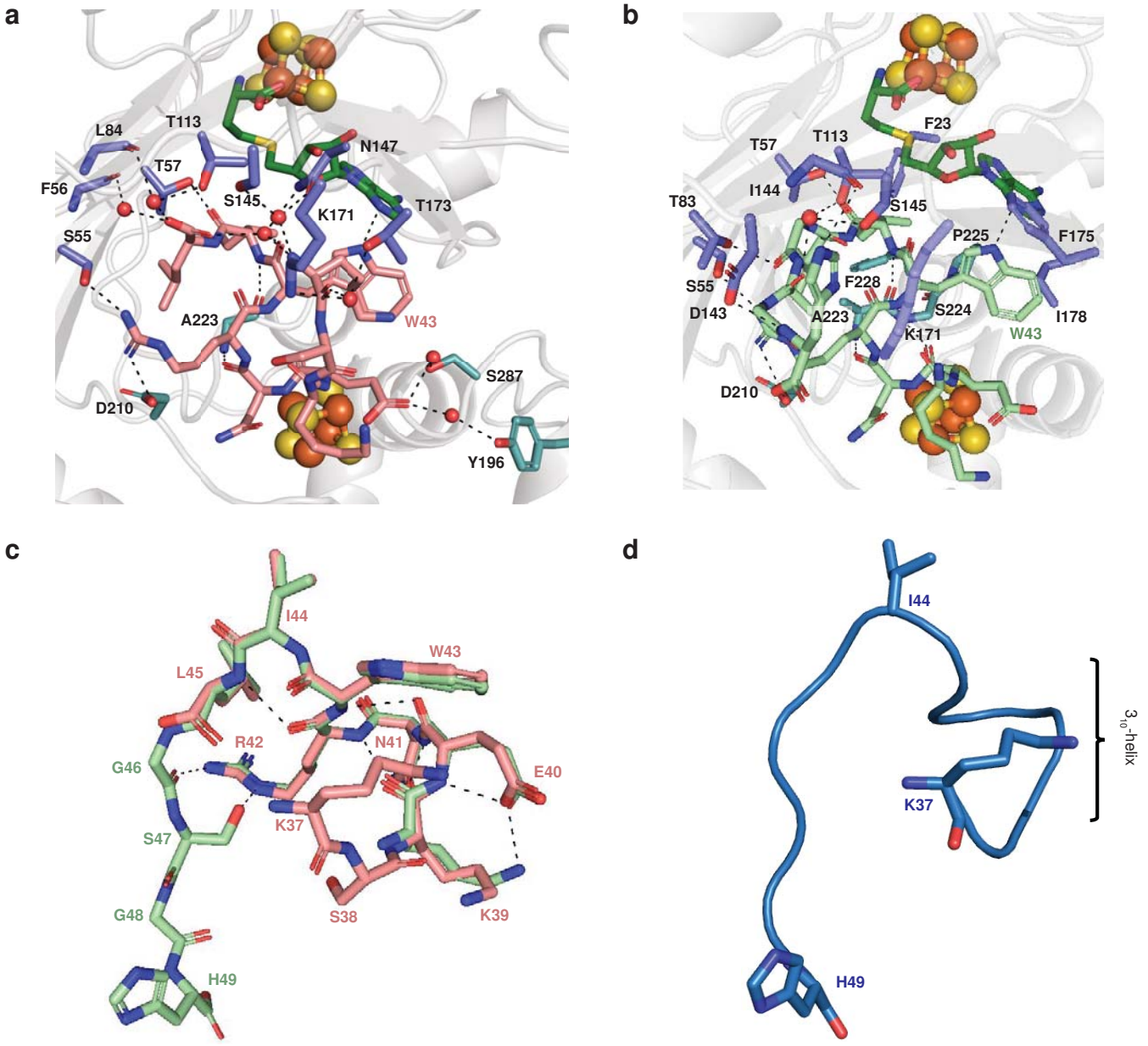
a
L84
T113
N147
T57
F56
S145
K171
T173
S55
A223
W43
S287
D210
Y196
b
F23
T57
T113
T83
I144
S145
P225
F175
S55
F228
D143
A223
S224
I178
K171
W43
D210
c
I44
W43
L45
R42
N41
G46
E40
K37
S47
G48
S38
K39
H49
d
I44
K37
H49
3$_{10}$-helix

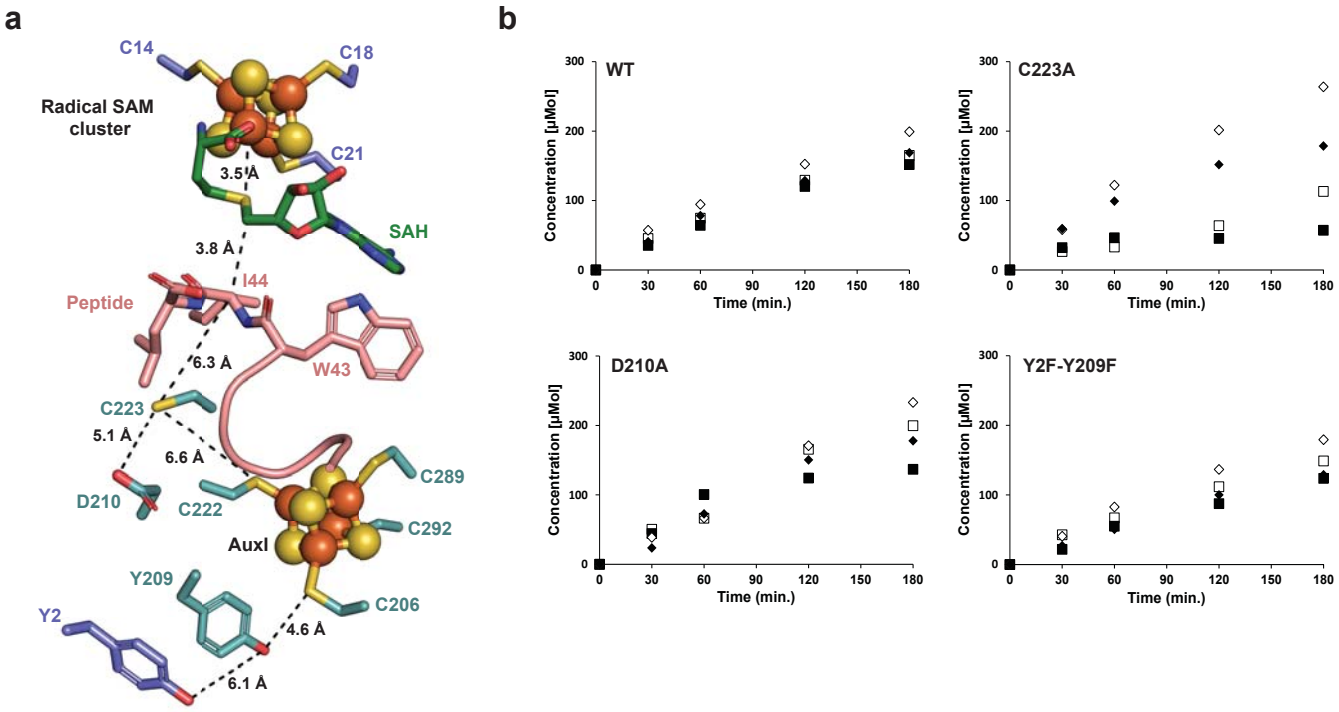
a
C14
C18
Radical SAM
cluster
C21
3.5 Å
SAH
3.8 Å
I44
Peptide
6.3 Å
W43
C223
5.1 Å
6.6 Å
C289
D210
C222
C292
AuxI
Y209
C206
Y2
4.6 Å
6.1 Å
b
WT
C223A
D210A
Y2F-Y209F
Concentration [µMol]
Time (min.)
0
30
60
90
120
150
180
100
200
300

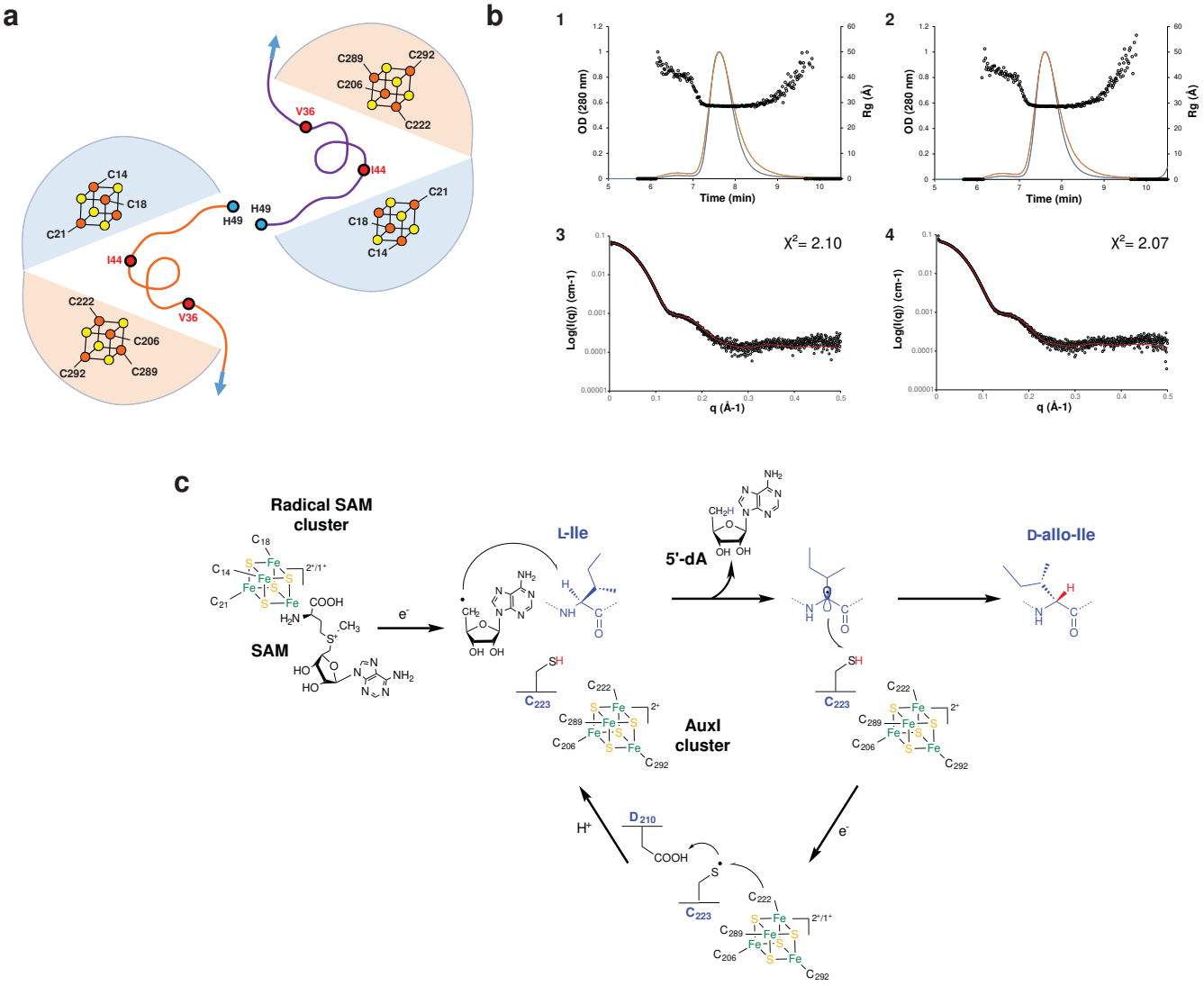
a
C289
C292
C206
C222
V36
I44
C14
C18
C21
H49
H49
C21
C18
C14
I44
V36
C222
C206
C292
C289
b
1
2
OD (280 nm)
Rg (Å)
Time (min)
3
4
X2= 2.10
X2= 2.07
Log(I(q)) (cm-1)
q (Å-1)
c
Radical SAM cluster
SAM
e-
L-Ile
5'-dA
D-allo-Ile
Auxl cluster
C223
H+
D210
e-